



Finite element modelling of bond–slip at anchorages of reinforced concrete members subjected to bending

Maruful Hasan Mazumder¹ · Raymond Ian Gilbert²

© Springer Nature Switzerland AG 2019

Abstract

The bond mechanism plays a decisive role when anchorage failure in a reinforced concrete (RC) member occurs. A refined model of bond–slip is therefore needed to analyse RC members by analytical or finite element (FE) modelling where the anchorage of reinforcement is critical, such as at a lapped-splice or in any situation where the strength of a bar is required to be developed to achieve its ultimate strength. This paper presents results of FE modelling of some experimental RC specimens with anchorage of deformed steel reinforcing bars in tension, including the cases of end development and lapped splices of bars in specimens subjected to bending. The FE modelling of the anchorage length specimens with bond–slip laws calibrated from experimental results was better able to predict the load–deflection behavior observed during experimental tests. A comparison of the results obtained using the calibrated bond–slip laws with those using conventional Fédération Internationale du Béton bond–slip laws is made and discussion is provided on the effects of the anchorage lengths and bar diameters on the bond–slip relationships.

Keywords Bond–slip · Reinforced concrete · Anchorage length · Finite element modelling

1 Introduction and background

The assumption of perfect bond between the concrete and reinforcing bar is often a sufficient assumption when modelling the ultimate behavior of a large reinforced concrete (RC) structure, but it is not of course appropriate when anchorage failure occurs. The bond mechanism affects the collapse load behavior of a structural member or parts of a structural member where anchorage of reinforcement is critical. The bond stress–slip law specified in the widely accepted Fédération Internationale du Béton (FIB) model code [1] is principally based on results of pull-out tests on reinforcement anchored in concrete for a very short length. However, the conditions favorable for the development of somewhat uniform bond stress in a short anchorage length of a RC test specimen are not representative of the conditions of bond stress in the longer

anchorage lengths of practical RC members. Local bond stress–slip relationship may become highly complex due to bond deterioration with splitting cracks in RC members [2]. Highly fluctuating bond stress conditions may arise within the anchorage lengths of bars in RC flexural members with the presence of cracks crossing the anchorage length [3].

Significant research efforts have been put into more realistic assessment and modelling of bond–slip in relatively long anchorage lengths in RC test specimens with conditions resembling those in practical RC members such as those in RC beam-column joints (e.g., [4, 5]) or in RC members with predominant flexural conditions (e.g., [3, 6–10]) with monotonic as well as cyclic load applications. Analytical modelling of bond–slip laws was undertaken by Mazumder [11] to assess the bond stress–slip relations along critical anchorage lengths

✉ Maruful Hasan Mazumder, maruf320@yahoo.com; mhasandee@cuet.ac.bd; Raymond Ian Gilbert, i.gilbert@unsw.edu.au | ¹Department of Disaster and Environmental Engineering, Chittagong University of Engineering and Technology, Raozan, Chittagong 4349, Bangladesh. ²School of Civil and Environmental Engineering, University of New South Wales, Sydney, NSW 2052, Australia.



of deformed steel bars in tension in some full-scale RC specimens subjected to bending. The analytical modelling results was compared with the test results [3, 7, 8] from experimental RC beam and slab specimens, referred to herein as anchorage length specimens, which included typical cases of end development (with development length l_d) and lapped splices (of length l_s) of deformed bars in tension. The anchorage length specimens were experimentally tested by the authors to determine average ultimate bond stress ($\tau_{avg,exp}$) calculated from the measured maximum load (P_{max}) at anchorage failure. The analytical modelling procedure proposed by Yankelevsky [12] was adapted by Mazumder [11] with a modified solution procedure to determine peak local bond stress (τ_y) and other constituent parameters of a representative bond-slip law for each of the selected anchorage length specimens. It was found that calibration of a conventional bond-slip model was required to reproduce bond zone conditions and local bond stresses within the anchorage of a selected specimen so that the calculated average ultimate bond stress ($\tau_{avg,cal}$) from the analytical model is in good agreement with that ($\tau_{avg,exp}$) observed during the experiment of the specimen.

The load-deflection behavior of the RC test specimens was also observed during the experiment up to the point of anchorage failure. This paper mainly aims at presenting results of finite element (FE) modelling [11] of some selected anchorage length specimens where the calibrated bond-slip laws were shown to simulate satisfactorily the collapse load behavior of the anchorage length specimens. A comparison of the results obtained using the calibrated bond-slip laws with those using the conventional FIB bond-slip law is also made in this paper and discussion is provided on the effects of the anchorage lengths and bar diameters on the bond-slip relationships.

2 Analytical modelling of bond-slip relations in RC members

The bond stress (τ) in RC members is dependent on the radial stress (σ_r) developed in the interfacial bond-slip layer through the effect (ϕ) of deformity of the reinforcing bar. This is demonstrated in the widely accepted bond-slip model of Goto [13] where an internally cracked bond-slip layer surrounding a bar is idealized by compression cones forming between internal cracks in concrete (Fig. 1). The radial stresses in the compression cones are directly affected by the parameters (τ - s) of the bond-slip model which in turn affects radial displacement (w) in concrete. The bond-slip action also affects the overall vertical deformation in RC members in bending. In the numerical modelling [14] of bond-slip behavior, this fundamental relationship is expressed as follows where E_i is a measure of the stiffness and β_r is the depth of the bond-slip layer.

$$\tau_u = -\sigma_r \tan \phi = E_i / \beta_r (\sin \phi \cdot \cos^2 \phi \Delta u - \cos^3 \phi \Delta w) \tag{1}$$

The analytical modelling [11] for the bond-slip behavior in the anchorage specimens was undertaken using the FIB bond-slip model [1] as a reference model. The model specifies local bond stress versus local slip relationships as statistical mean curves for a broad range of cases of confined and unconfined concrete, and the relationships are valid for short anchorage lengths only under well-defined conditions. The bond-slip laws, as applicable for two different bond failure types, are defined by five equations (Eqs. 2-6) with parameters and parametric values shown in Fig. 2 and Table 1 [1]. A maximum of four bond zones (Zone I-IV, as shown in Fig. 2) exist in the bond-slip law for the pull-out type bond failure. Two types of bond-slip laws can be defined for the splitting type bond failure in a specific bond condition, one is for unconfined anchorage conditions in concrete ($K_{tr} = 0$) and the other is for confined anchorage conditions with stirrups. With $s_1 = s_2$, and

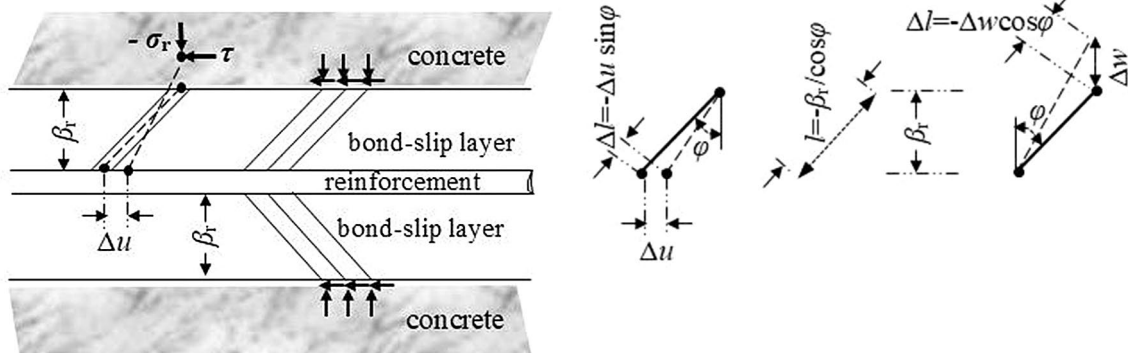


Fig. 1 Bond-slip model—the relation between Δu , Δw , τ and σ_r [14]

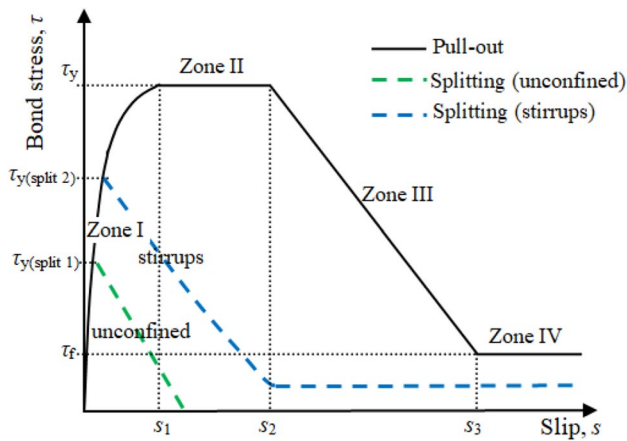


Fig. 2 Analytical bond stress–slip relationship for monotonic loading. Adopted from [1]

$\tau_f = 0$ for the unconfined anchorage condition, there are two bond zones (Zone I and III, as shown in Fig. 2) in the bond–slip law whereas three bond zones may exist in the bond–slip law for the confined anchorage condition (with $s_1 = s_2$, and $\tau_f = 0.4\tau_y$).

$$\tau = \tau_y (s/s_1)^\alpha \quad \text{for } 0 \leq s \leq s_1 \tag{2}$$

$$\tau = \tau_y \quad \text{for } s_1 \leq s \leq s_2 \tag{3}$$

$$\tau = \tau_y - (\tau_y - \tau_f)(s - s_2)/(s_3 - s_2) \quad \text{for } s_2 \leq s \leq s_3 \tag{4}$$

$$\tau = \tau_f \quad \text{for } s_3 < s \tag{5}$$

The expression for τ_y for splitting type bond failures is given by Eq. (6) where $\eta_2 = 1.0$ for good bond conditions and 0.7 for all other cases; f'_c is the characteristic (cylinder) compressive strength of concrete, c_{max} and c_d are the maximum and minimum available concrete cover for a bar to its nearest concrete surface, and K_{tr} is a factor that accounts for the

effects of the passive confinement. The subscript 1 at $\tau_{y(split)}$ is to denote the value of τ_y for the splitting type bond failure in unconfined concrete ($K_{tr} = 0$), while the subscript 2 at $\tau_{y(split)}$ is for the same in confined concrete (with specified K_{tr}).

$$\tau_{y(split1,2)} = \eta_2 \cdot 6.54 \cdot (f'_c/20)^{0.25} (20/d_b)^{0.20} \left[(c_d/d_b)^{0.33} (c_{max}/c_d)^{0.1} + 8K_{tr} \right] \tag{6}$$

The formulation of typical analytical and numerical models for bond–slip is based upon the assumption that the influence of concrete deformation on slip is negligible, especially when bond failure occurs with strain in the reinforcing bars being below the yield strain [12]. With this simplified assumption, the local bond stress for a bar of circular cross-section, $\tau(x)$ can be related to slip, $s(x)$ according to the following expression

$$\tau(x) = \frac{E_s d_b}{4} \cdot \frac{d^2 s(x)}{dx^2} \tag{7}$$

where E_s is the modulus of elasticity of steel. The typically nonlinear bond stress–slip relationships can be idealized by linear relationships (including the Zone I) and second-order linear differential equations for the different bond zones can be defined [12]. This linear approximation of bond–slip laws is computationally more viable in FE model simulations [15] compared to the nonlinear approximations of the same [16–19]. Therefore, a linear relationship between bond stress and slip can be conveniently used to replace $\tau(x)$ in Eq. (7) by $s(x)$ and the differential equations for the different bond zones can be defined in terms of $s(x)$. The solution of the differential equations yields the expressions for slip and variations of strain (ϵ_x) for different bond zones of a bond–slip law. The boundary conditions that are imposed in the solution are

$$\epsilon_x = 0 \quad \text{at } x = 0 \tag{8}$$

$$\epsilon_x = \epsilon_o \quad \text{at } x = l_d \tag{9}$$

Table 1 Parameters for defining mean bond stress–slip relationships of deformed bars (according to [1])

Parameters (1)	Pull-out		Splitting			
	$\epsilon_s < \epsilon_{s,y}$		$\epsilon_s < \epsilon_{s,y}$			
	Good bond condition (2)	All other bond condition (3)	Good bond condition		All other bond conditions	
			Unconfined (4)	Stirrups (5)	Unconfined (6)	Stirrups (7)
τ_y	$2.5\sqrt{f'_c}$	$1.25\sqrt{f'_c}$	$7.0 (f'_c/20)^{0.25}$	$8.0 (f'_c/20)^{0.25}$	$7.0 (f'_c/20)^{0.25}$	$8.0 (f'_c/20)^{0.25}$
s_1	1.0 mm	1.8 mm	$s(\tau_y)$	$s(\tau_y)$	$s(\tau_y)$	$s(\tau_y)$
s_2	2.0 mm	3.6 mm	s_1	s_1	s_1	s_1
s_3	c_{clear}^a	c_{clear}^a	$1.2s_1$	$0.5c_{clear}^a$	$1.2s_1$	$0.5c_{clear}^a$
α	0.4	0.4	0.4	0.4	0.4	0.4
τ_f	$0.40\tau_y$	$0.40\tau_y$	0	$0.4\tau_y$	0	$0.40\tau_y$

^a c_{clear} (or r_b) is the clear distance between ribs

where ϵ_0 is the strain calculated from the bar stress based on the analysis of cracked section at $x=l_d$. With specified boundary conditions and compatibility conditions of bond stress, strain and slip between two adjacent bond zones, the equations can be solved [12] to find unknown lengths of different bond zones and constants of the solutions for $s(x)$ for a chosen bond-slip law in an anchorage length specimen.

2.1 Analytical modelling and solutions for calibrating bond-slip of anchorage length specimens

With a few modifications of its mathematical formulations and solutions, the analytical model proposed by Yankelovsky [12] was used by Mazumder [11] to determine representative values of constituent parameters (τ_y, s_1, s_2 or s_3) in a trial and error method for calibrating bond-slip laws for some selected anchorage length specimens (specified therein as DL-1, DL-3, DL-6, DL-7 and DL-8 for end development and BL-2, BL-5 and BL-9 for lapped splice specimens). From the observations of the type of bond failure in the specimens, it was assumed that two bond zones (for splitting type bond failure) should ideally exist in the representative bond-slip laws for most of the anchorage length specimens (except for BL-5 with three bond zones). With a chosen bond-slip law for an anchorage length specimen, the unknown lengths of bond zones within the anchorage could be determined (x_y for DL-1 and DL-3, as shown in Fig. 3) by the analytical solution procedure [11] and subsequently, local bond stresses could be determined for

corresponding values of $s(x)$. With appropriate parametric values of a bond-slip law for an anchorage length specimen (e.g., FIB bond-slip law for DL-1) derived from respective material parameters, four equations containing four unknowns (including constants of equations) were solved to find unknown length (x_y) of a bond zone. However, the analytical modelling [12] can be used to derive solutions for the arbitrary bond-slip law (pull-out or splitting) chosen for any anchorage length specimen. The solutions can be found by manual calculations or using optimization algorithm for solution [11] with reasonable input values of the unknowns.

With the chosen FIB bond-slip laws for different anchorage length specimens, no practical solution ($x_y < l_d$) of the unknown bond zone length could be found for the selected specimens except for DL-1. However, real solutions of the unknown bond zone lengths for the selected anchorage length specimens could be determined using a revised bond-slip law reasonably calibrated from measurements made in the experimental program [3, 7, 8]. The calibrated bond-slip laws for each of the selected specimens are shown in Table 2.

The experimentally measured end slip of the debonded bars at P_{max} was used to decide reasonable initial values of the slips s_1 or s_2 in Fig. 2 and the post-peak end slip of the bars at $0.4P_{max}$ gave an indication of the spread of the tail end (s_3) of a bond-slip law chosen for the analytical modelling procedure. Since more than one set of real solutions of unknowns for a specimen could be determined for different bond-slip laws, further analyses were performed using them to calculate the local bond stress at locations of the

Fig. 3 Idealization of bond zones within the anchorage of selected anchorage length slab specimen

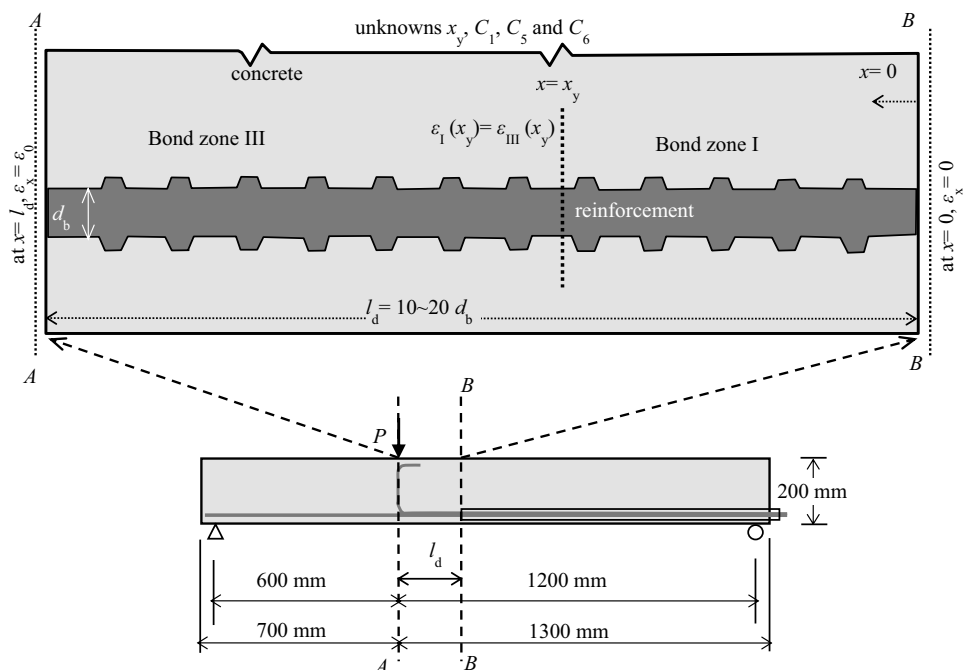


Table 2 Calibrated bond–slip laws for selected specimens and results of analytical modelling

Specimens (bond–slip laws) (1)	Constitutive parameters of bond–slip laws (confined/unconfined, good bond condition) $\epsilon_s < \epsilon_{s,y}$ (2)						Bond zone length (x_y, x_2) (mm) (3)	Average bond stress within anchorage τ_{avg} (MPa) (4)	Structural and material parameters (5)
	τ_y (MPa)	s_1 (mm)	s_2 (mm)	s_3 (mm)	α	τ_f (MPa)			
DL-1, $l_d = 10d_b$ (calibrated)	8.80	0.25	0.25	3	0.4	0	$x_y = 119.7$	$\tau_{avg,exp} = 7.69$ $\tau_{avg,cal} = 7.72$	$d_b = 16$ mm; $c = 25$ mm;
DL-3, $l_d = 20d_b$ (calibrated)	6.20	0.8	0.8	$10 (\approx r_b)^a$	0.4	0	$x_y = 145.1$	$\tau_{avg,exp} = 5.98$ $\tau_{avg,cal} = 5.98$	$c_{max} = 60$ mm; $f'_c = 38.5$ MPa; $f_{sy} = 546$ MPa
DL-1 and 3 (FIB bond–slip law)	10.19	0.35	0.35	0.42	0.4	0	$x_y = 107.2$ (DL-1)	$\tau_{avg,exp} = 7.69$ $\tau_{avg,cal} = 7.51$	
DL-6, $l_d = 10d_b$ (calibrated)	12.80	0.40	0.40	4	0.4	0	$x_y = 80.9$	$\tau_{avg,exp} = 11.92$ $\tau_{avg,cal} = 11.90$	$d_b = 12$ mm; $c = 25$ mm;
DL-7, $l_d = 15d_b$ (calibrated)	10.40	0.6	0.6	6	0.4	0	$x_y = 132.3$	$\tau_{avg,exp} = 9.41$ $\tau_{avg,cal} = 9.35$	$c_{max} = 60$ mm; $f'_c = 38.5$ MPa;
DL-8, $l_d = 20d_b$ (calibrated)	9.00	0.7	0.7	$7 (\approx r_b)^a$	0.4	0	$x_y = 234.8$	$\tau_{avg,exp} = 6.72$ $\tau_{avg,cal} = 6.72$	$f_{sy} = 561$ MPa
DL-6 to 8 (FIB bond–slip law)	11.86	0.51	0.51	0.61	0.4	0	No real solution	–	
BL-2, $d_b = 20$ mm, $l_s = 400$ mm; unconfined (calibrated)	4.85	0.5	0.5	1	0.4	0	$x_y = 100$	$\tau_{avg,exp} = 3.87$ $\tau_{avg,cal} = 3.84$	$c = 25$ mm; $c_{max} = 70$ mm; $A_{tr}/s = 1.57$; $K_{tr} = 3.9\%$;
BL-5, $d_b = 20$ mm, $l_s = 300$ mm; confined (calibrated)	7.00	0.5	0.6	0.8	0.4	2.0	$x_y = 95.9$ $x_2 = 206.2$ (3 bond zones)	$\tau_{avg,exp} = 4.51$ $\tau_{avg,cal} = 4.50$	$f'_c = 43.0$ MPa (for BL-2 and BL-5) and 36.1 MPa for BL-9;
BL-9, $d_b = 20$ mm, $l_s = 400$ mm; confined (calibrated)	5.35	0.5	0.5	5.0	0.4	0	$x_y = 220.5$	$\tau_{avg,exp} = 4.89$ $\tau_{avg,cal} = 4.89$	$f_{sy} = 534$ MPa
BL-2, 5, 9 (FIB bond–slip law)	$\tau_{y(split\ 1,2)}$ are 4.84 MPa for BL-2, 7.03 MPa for BL-5 and 5.34 MPa for BL-9								

^a r_b is the rib spacing

ribs of the reinforcement within the anchorage length (l_d or l_s) of each specimen. The average of the calculated local bond stresses ($\tau_{avg,cal}$) at P_{max} was compared for consistency with the experimentally determined average ultimate bond stress ($\tau_{avg,exp}$) for that specimen.

The experimental anchorage length slab specimens with end development of bars had dimensions of 2000 mm × 600 mm × 200 mm and the beam specimens with lapped splice bars (BL-2, 5, 9) had dimensions 2.3 m long, 250 mm wide and 300 mm high. The anchorage lengths of the different specimens are given in column 1 of Table 2 and structural and material parameters of the specimens are provided in column 5 of the same table. It may be observed that the FIB bond–slip laws for anchorage length specimens (e.g., for DL-1 and DL-3 in Table 2) with identical structural and material parameters for a bar are the same regardless of the variations of the anchorage lengths. The calibrated bond–slip laws for the various specimens, however, are found to vary significantly. While the FIB bond–slip laws showed minor variations between the anchorage specimens with different bar sizes (e.g., for $d_b = 16$ mm and $d_b = 12$ mm), the calibrated bond–slip

laws are found to be significantly different. This indicates that variations of anchorage lengths and bar diameters significantly affect the bond–slip laws for anchored bars in practical RC members.

3 Finite element modelling of the anchorage length specimens

The efficacy of a FIB bond–slip law and of a calibrated bond–slip law for a specimen was further examined using FE modelling [1] to simulate the behavior of the laboratory test specimens, including load–deformation characteristics, failure load, crack development and progression. Three dimensional (3D) FE modelling was undertaken in order to compare the effects of using the analytically calibrated bond–slip laws and the specified FIB bond–slip laws for modelling the RC specimens. The FE modelling software Atena-v.4.2.7 [20] was used. The effects of varying the bond–slip laws and other associated model parameters on the load versus vertical deflection (Δ) behavior of some selected anchorage length specimens were assessed.

The observed load–deflection behavior of an anchorage length specimen was simulated by implementing chosen bond–slip laws in a 3D FE model of each of the selected test specimens.

3.1 Materials and methods for FE modelling of anchorage length specimens

The FE model simulations were carried out within the framework of the 3D FE modelling software Atena-v.4.2.7 [20] where it was necessary to input a bond–slip law to control the bond behavior at the interface between concrete and reinforcement. The complete FE (structural) modelling of the test set-up of a selected specimen was done by combining a number of macro-elements formulated in the Atena pre-processor interface. The geometry of the macro-elements was specified by inputting appropriate coordinates to define the structure. The geometry of the macro-element used to model the concrete was defined by inputting the coordinates of the eight corner points of the 3D element as shown in Fig. 4. The coordinates for the loading plate and the two supports were also specified according to the practical dimensions of those elements used during the experiment [3, 7, 8]. The reinforcing bars embedded within the concrete were also implemented by appropriately inputting the co-ordinates for each bar. Load and restraints to different degrees of freedom (DOF) were applied at appropriate points of load application and at the two supports as shown in the Fig. 4.

The dimensions, geometry, material properties, constitutive material models and the loading arrangement in the FE model of an anchorage length specimen were implemented in compliance with those of the practical test specimen. The material model chosen for the concrete was a fracture-plastic constitutive model [20]. The concrete

material model combines constitutive models for (tensile) fracturing and compressive (plastic) behavior. The fracture model for concrete employs Rankine failure criterion and exponential softening and it can be implemented with either a rotating or a fixed crack model. The input material properties for the concrete and reinforcement of the model were the same as measured at the time of testing the specimens (column 5 of Table 2). The fracture energy of concrete (G_F) was estimated according to the equation given by Vos [21]. The loading and support conditions in the laboratory tests were simulated in the FE analyses.

The mesh discretisation for the concrete macro-element was appropriately chosen to ensure reasonably accurate simulation while keeping the model as simple as possible. Since, the determination of the vertical deflection at the monitoring point was the principal concern rather than the determination of stresses at any point within the concrete macro-element, 3D isoparametric brick elements for concrete were considered to be sufficient to yield reasonably accurate results while maintaining a simpler mesh discretisation than would have been possible using other types of finite elements for concrete. Application of the bond model with relatively coarse meshes for the concrete elements is important to avoid some numerical problems during FE modelling of RC specimens. Instead of the slip of the interface between steel bar and surrounding concrete, the bond behavior may be captured by cracking of the surrounding concrete with smaller mesh size in the vicinity of the reinforcing bar approaching the bar diameter [22]. Therefore, the discretisation of meshes for the concrete macro-elements in the anchorage length slab specimens was done with five elements to cover the thickness of the slab specimen which was considered sufficient to yield reasonably accurate results during the FE simulation. The interfaces between the various elements, including the

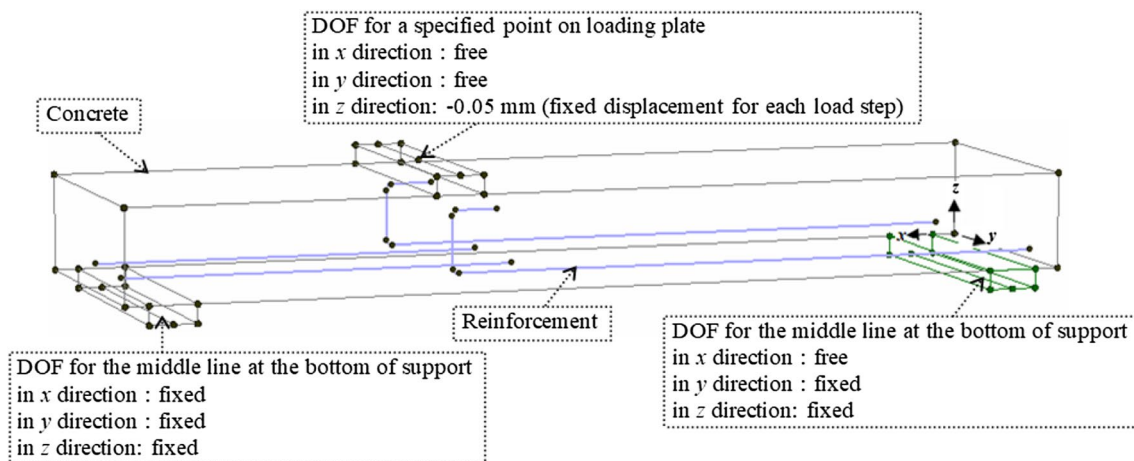


Fig. 4 Coordinates, load and restraints in the FE model of a test (slab) specimen

interfaces between the concrete and reinforcement, the concrete and the support plates and the concrete and the loading plate, were automatically generated with the default settings in the Atena software. The mesh discretisation of the loading and the support plates (steel plates) in the Atena FE model was generated as default in the Atena software, but was checked for compatibility at the common nodes of their contact points with the concrete macro-elements. Figure 5a shows the skeleton of the FE model of an anchorage length slab specimen including the monitoring point of vertical deflection specified with coordinates provided as input in the Atena FE model. Figure 5b shows the finite element mesh adopted for the analyses. Figure 6 shows the skeleton of the FE model and mesh adopted for the lapped splice beam specimen (BL-2).

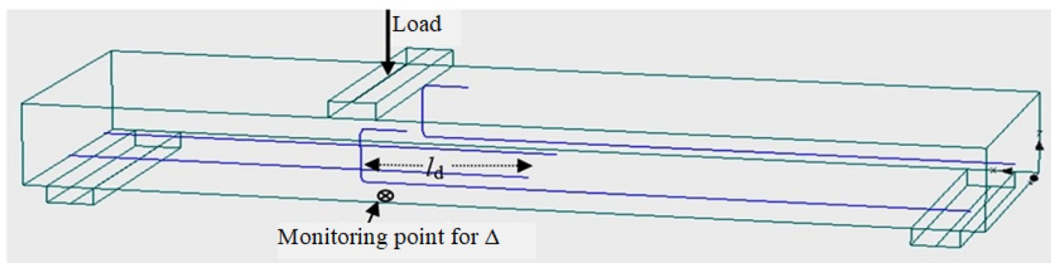
Reinforcement bars were embedded within concrete macro-element by inputting its geometric locations in the model in global coordinates. The pre-processing routine of the Atena program decomposed reinforcing bars into individual truss elements embedded into solid elements of concrete. The steel stress–strain properties of the embedded truss elements are typically linked to concrete elements through fictitious interface of bond-link elements [22–25]. The interface is automatically introduced on the material level in most FE modelling programs or packages. The 3D FE modelling system of Atena essentially includes three types of finite elements: concrete continuum elements (3D), bar truss elements (constant strain) and automatically introduced bond-link elements (constant slip).

The nodal displacement formulation for the embedded bar elements in Atena is extended to include a bond element with its new degree of freedom s representing bond slip, which is the difference between concrete and bar displacements on the element boundary. The slip degree of freedom (s) is accordingly introduced into the expression for stress evaluation of a bar element. During the FE model simulation with Atena, the inner iterative process for reinforcement continues until achieving acceptably low out-of-balance forces that are searched according to the slip of the linked bond element [22].

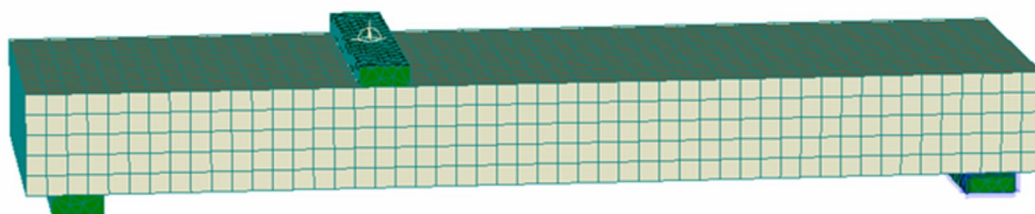
Load was applied by imposing small displacements. The analytically calibrated bond–slip law and the FIB bond–slip law were used as input parameters for the bond in two separate FE models of the specimens while keeping other model parameters the same. The load–deflection curves obtained from the FE models were compared with the respective load–deflection response that was observed in the laboratory.

4 Results and discussion

Since the FIB bond–slip laws are commonly used for modelling RC members where anchorage of reinforcement is critical, the discussion on analytical and FE modelling results is made using FIB bond–slip laws as a reference model. The qualitative and quantitative differences between the bond–slip law specified in the FIB model

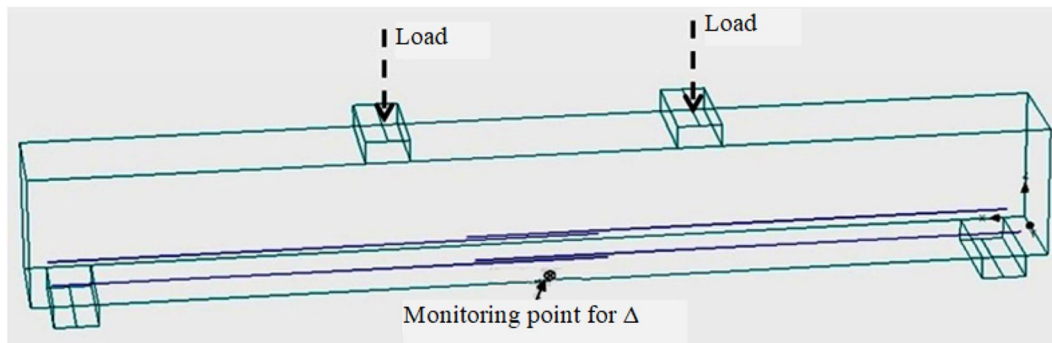


(a) Skeleton of a FE model of an anchorage length specimen

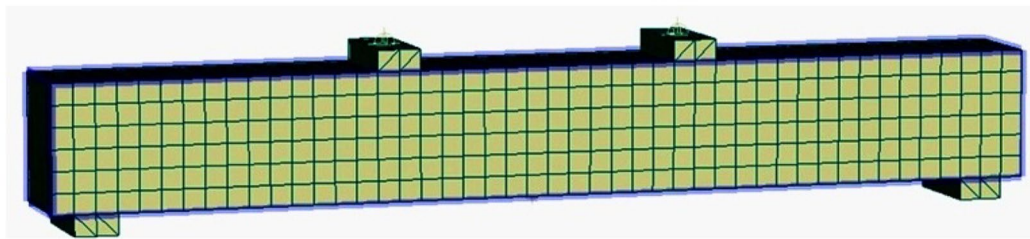


(b) Concrete elements and supports of the FE model

Fig. 5 FE model of an anchorage length specimen ($d_b = 16$ mm; $l_d = 10/20d_b$)



(a) Skeleton of a FE model of a lapped splice beam specimen (BL-2)



(b) Concrete elements and support of the FE model of BL-2

Fig. 6 FE model of a lapped splice beam specimen ($d_b = 20$ mm; $l_s = 20 d_b$)

code or specifications [1] and the bond–slip laws analytically calibrated to accurately model the behavior of the anchorage conditions tested in the laboratory are discussed. However, the discussion in this section is principally focused on the FE model outputs and demonstrates the significant improvement obtained by using the calibrated bond–slip laws in the FE modelling.

4.1 Limitations of the conventional analytical bond–slip laws

The limitation of the conventional bond–slip laws for anchorage in RC members is that the effect of concrete deformation on bond stresses is neglected, as is commonly assumed when the steel strain is less than the yield strain, $\epsilon_s < \epsilon_{s,y}$. However, the concrete deformation is expected to vary depending on the variations of anchorage lengths or bar diameters. If there were no influence of concrete deformation on bond stresses, the average ultimate bond stresses would be the same for identical specimens (where the same materials are used in the same structural geometry) regardless of the variation of anchorage lengths. The bond–slip laws according to the FIB design model for the identical anchorage length specimens (e.g. for DL-1 and DL-3, in Table 2) are, in fact, the same regardless of the variations of the anchorage lengths or bar diameters whereas the constituent parameters of the calibrated

bond–slip laws are found to be different for variable anchorage lengths or bar diameters in otherwise identical specimens. Therefore, the required changes of the constitutive parameters of the bond–slip laws for each specimen indirectly accounts for the effect of concrete deformation on bond stresses. Table 2 also shows that the constituent parameters of some of the calibrated bond–slip laws are significantly different from the FIB bond–slip laws for the respective specimens (e.g. the parameters for DL-3, DL-8 and DL-10).

4.2 Results of FE modelling of the anchorage length specimens

The calibration of the FE models of the anchorage length specimens was mainly aimed at achieving the load–deflection behavior close to that observed during the experiment. During the FE model calibration, the input value of the fracture energy (G_F) of concrete was found to dominate the load carrying capacity of the structure. Figure 7 shows the comparison of the experimental results of load–deflection behavior with that of the FE models for DL-3 for three different input values of G_F , using the bond–slip laws specified according to FIB MC-10. Although the maximum load observed in the laboratory could be achieved by adjusting the value of G_F , the observed vertical deflection (Δ) at P_{max} could not

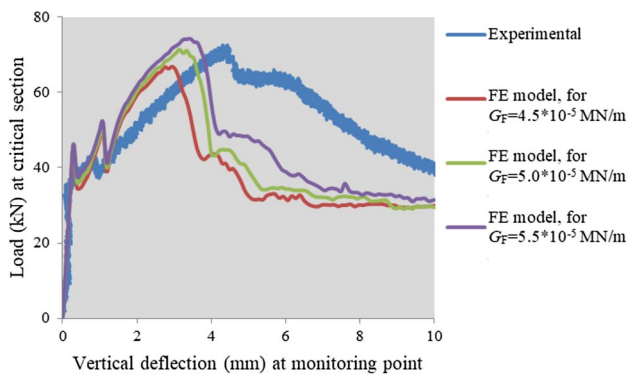


Fig. 7 Load–deflection behavior of the experimental and FE models of DL-3 (for variable G_F)

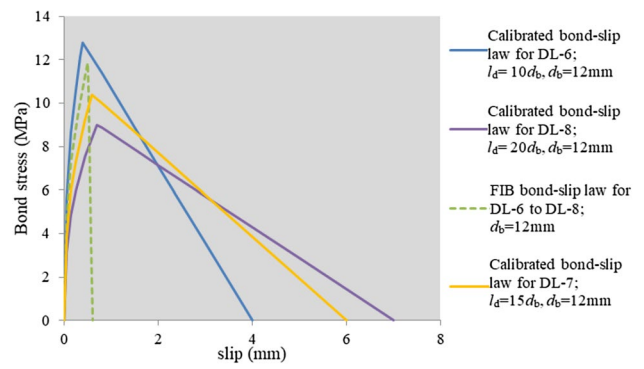


Fig. 9 Calibrated and the respective FIB bond–slip laws (for DL-6 to DL-8) used for the FE modelling

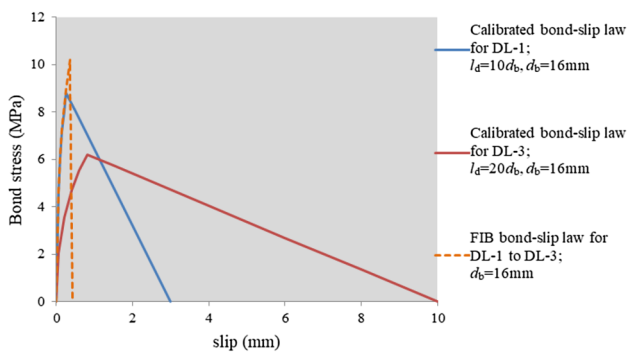


Fig. 8 Calibrated and the respective FIB bond–slip laws (for DL-1 to DL-3) used for the FE modelling

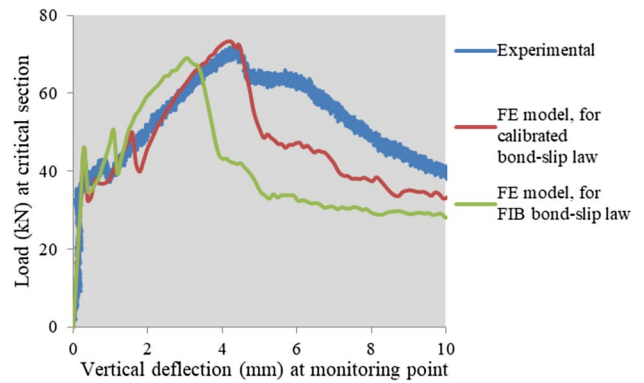


Fig. 10 Load–deflection of experimental specimen and FE models of DL-3

be achieved with the changes of G_F alone. The bond–slip law had to be adjusted simultaneously with G_F to achieve the observed vertical deflection at P_{max} by trial and error FE model simulations.

The calibrated bond–slip laws that were used for FE modelling of the selected anchorage specimens with end development of bars (for DL-1, DL-3 and DL-6 to DL-8) are shown in Figs. 8 and 9. The respective FIB bond–slip laws for the anchorage specimens are also shown in the figures. Significant differences between the analytically calibrated bond–slip laws for the specimens and the respective FIB bond–slip laws are evident especially for the longer anchorage length specimens (e.g. for $l_d = 20d_b$).

A reasonable prediction of the vertical deflection of the anchorage length specimens could be achieved using the FE model with the analytically calibrated bond–slip laws. Figure 10 for DL-3 compares the FE model outputs of load–deflection using the specified FIB bond–slip laws and the analytically calibrated bond–slip laws (Table 2). Figure 11 shows the FE model output of the load–deflection using the specified FIB and the analytically calibrated bond–slip laws for a lapped splice beam (BL-2).

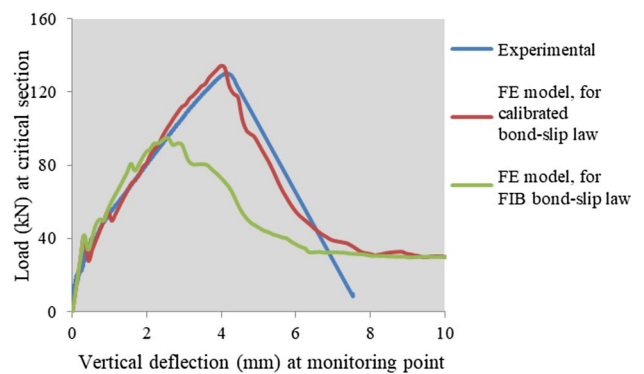


Fig. 11 Load–deflection of experimental specimen and FE models of BL-2

The comparison of the FE modelling results of load–deflection responses of specimens DL-3 and BL-2 shows that significant improvement is obtained by using the calibrated bond–slip laws compared to the FIB laws. Being reasonably representative of the true slips under different magnitudes of local bond stresses along the

anchorage, the calibrated bond–slip models resulted in good agreement with the observed vertical deflection behavior of the specimens under loads. It was observed during the practical experiments that the splitting induced pull-out type bond failures progressed slowly for the specimens with the longer anchorages in contrast to the sudden splitting type bond failures that were typical of the specimens with the short anchorage lengths.

5 Conclusions

Analytical modelling of bond–slip laws was undertaken to calibrate local bond stress–slip relations along the anchorage lengths of deformed steel reinforcing bars in tension, including selected cases of end development and lapped splices of bars in some full-scale RC specimens subjected to bending. A viable analytical modelling procedure was used assuming linear approximation of a bond–slip law using constituent parameters reasonably based on experimental observations of each selected anchorage length specimen. It was found that recalibration of a conventional FIB bond–slip model was required to reproduce bond zone conditions and local bond stresses within the anchorage length of a specimen so that the calculated average ultimate bond stress from the analytical model solution is in good agreement with that observed during the laboratory testing.

The calibrated bond–slip laws and the FIB bond–slip relations were implemented in 3D FE models of selected anchorage length specimens. A comparison of the FE modelling results obtained using the calibrated bond–slip laws with those using the FIB bond–slip law is made in this paper. The FE modelling of the anchorage specimens with calibrated bond–slip laws was better able to predict the vertical deflection of a specimen at maximum load. The calibrated bond–slip laws for the anchorage specimens are also found to be significantly different from the FIB bond–slip laws for those specimens. Therefore, conventional bond–slip models need to be calibrated to account for the effects of the anchorage lengths and bar diameters on the bond–slip relationships.

Acknowledgements The experimental work of the research project (Ph.D.) was undertaken with the financial support of the Australian Research Council (ARC) through an ARC Discovery grant to the second author. FE modelling and analyses with Atena software were carried out at the computer laboratory of the School of Civil and Environmental Engineering of UNSW, Sydney, Australia. These supports are gratefully acknowledged.

Funding The experimental work of the research project was undertaken with the financial support of the Australian Research Council (ARC) through an ARC Discovery grant to the second author. The ARC Discovery (DP1096560) grant was given for the project entitled

‘Anchorage of reinforcement in concrete structures subjected to loading and environmental extremes’ for 3 years duration (2010–2012) of the project.

Compliance with ethical standards

Conflict of interest On behalf of the authors, the corresponding author states that there is no conflict of interest.

References

1. FIB (2012) Model code 2010 final draft, FIB MC-10: 2012. international federation for structural concrete (FIB—Fédération Internationale du Béton), Lausanne, Switzerland
2. Murcia-Delso J, Shing PB (2015) Bond–slip model for detailed finite-element analysis of reinforced concrete structures. *J Struct Eng ASCE* 141(4):04014125
3. Gilbert RI, Mazumder M, Chang ZT (2012) Bond, slip and cracking within the anchorage of deformed reinforcing bars in tension. In: 4th International symposium on bond in concrete, Brescia, Italy, June 2012
4. Wang S, Kang SB, Tan KH (2019) Evaluation of bond–slip behaviour of embedded rebars through control field equations. *Mag Concrete Res* 71(17):907–919
5. Sezen H, Moehle JP (2003) Bond–slip behaviour of reinforced concrete members. In: Proceedings of FIB symposium on concrete structures in seismic regions, CEB-FIP, Athens, Greece, 2003
6. Gilbert RI, Chang ZT, Mazumder M (2011) Anchorage of reinforcement in concrete structures subjected to cyclic loading. In: CONCRETE 11, 25th biennial conference of Concrete Institute of Australia, Perth, Australia, October 2011
7. Mazumder MH, Gilbert RI, Chang ZT (2012) A reassessment of the analysis provisions for bond and anchorage length of deformed reinforcing bars in tension. *Bonfring Int J Ind Eng Manag Sci* 2(4):1–8
8. Mazumder MH, Gilbert RI, Chang ZT (2013) Analytical modelling of average bond stress within the anchorage of tensile reinforcing bars in reinforced concrete members. *Int J Civ Environ Eng* 7(6):392–398
9. Ashtiani MS, Dhakal RP, Scott AN, Bull DK (2013) Cyclic beam bending test for assessment of bond–slip behaviour. *Eng Struct* 56:1684–1697
10. Liang X, Sritharan S (2014) An investigation of bond–slip behaviour of reinforcing steel subjected to inelastic strains. In: Tenth U.S. National conference on earthquake engineering, frontiers of earthquake engineering, Anchorage, Alaska, July 2014
11. Mazumder MH (2014) The anchorage of deformed bars in reinforced concrete members subjected to bending. Ph.D. thesis, University of New South Wales, Kensington, NSW, Australia
12. Yankelevsky DZ (1985) Analytical model for bond–slip behaviour under monotonic loading. *Build Environ* 20(3):163–168
13. Goto Y (1971) Cracks formed in concrete around deformed tension bars. *ACI J* 68(4):244–251
14. de Groot AK, Kusters GMA, Monnier T (1981) Numerical modeling of bond–slip behaviour. *HERON* 26(1B):1–90
15. Yankelevsky DZ (1985) New finite element for bond–slip analysis. *J Struct Eng ASCE* 111(7):1533–1542
16. Allwood RJ, Bajarwan AA (1996) Modeling nonlinear bond–slip behaviour for finite element analyses of reinforced concrete structures. *ACI Struct J* 93:539–544
17. den Uijl JA, Bigaj AJ (1996) A bond model for ribbed bars based on concrete confinement. *HERON* 41(3):201–226

18. Eligehausen R, Popov EP, Bertero VV (1983) Local bond stress–slip relationships of deformed bars under generalized excitations. Research report UCB/EERC-83/23, Earthquake Engineering Research Center, University of California, Berkeley
19. Lundgren K, Gylltoft K (2000) A model for the bond between concrete and reinforcement. *Mag Concrete Res* 52(1):53–63
20. Atena-v.4.2.7 (2009) Program documentation-part 1, atena theory manual. Cervenka consulting, Praha 5, Czech Republic
21. Vos E (1983) Influence of loading rate and radial pressure on bond in reinforced concrete: a numerical and experimental approach. Research report, Delft University Press, Netherlands
22. Jendele L, Cervenka J (2006) Finite element modelling of reinforcement with bond. *Comput Struct* 84:1780–1791
23. Allwood RJ, Bajarwan AA (1989) A new method for modelling reinforcement and bond in finite element analyses of reinforced concrete. *Int J Numer Methods Eng* 28:833–844
24. Elwi AE, Hrudey TM (1989) Finite element modelling for curved embedded reinforcement. *J Eng Mech ASCE* 115:740–754
25. Hartl H, Handel C (2002) 3D finite element modeling of reinforced concrete structures. FIB 2002, Osaka Congress, Japan

Publisher's Note Springer Nature remains neutral with regard to jurisdictional claims in published maps and institutional affiliations.